Biochimica et Biophysica Acta 1808 (2011) 2789–2797

Contents lists available at SciVerse ScienceDirect

Biochimica et Biophysica Acta

journal homepage: www.elsevier.com/locate/bbamem

# Electrophysiological properties of heteromeric TRPV4–C1 channels

Xin Ma [a,b,c], Bernd Nilius [d], Judy Wei-Yan Wong [a,b], Yu Huang [a,b], Xiaoqiang Yao [a,b,*]

[a] Li Ka Shing Institute of Health Sciences, The Chinese University of Hong Kong, Hong Kong, China
[b] School of Biomedical Sciences, The Chinese University of Hong Kong, Hong Kong, China
[c] Department of Cellular and Molecular Pharmacology, School of Medicine and Pharmaceutics, Jiangnan University, Wuxi, China
[d] Laboratory Ion Channel Research, KU Leuven, Leuven, Belgium

ARTICLE INFO

*Article history:*
Received 6 April 2011
Received in revised form 30 June 2011
Accepted 18 July 2011
Available online 18 August 2011

*Keywords:*
TRPV4–C1
Heteromeric channel
Cation permeability profile

ABSTRACT

We previously reported that TRPV4 and TRPC1 can co-assemble to form heteromeric TRPV4–C1 channels [12]. In the present study, we characterized some basic electrophysiological properties of heteromeric TRPV4–C1 channels. 4α-Phorbol 12,13-didecanoate (4α-PDD, a TRPV4 agonist) activated a single channel current in HEK293 cells co-expressing TRPV4 and TRPC1. The activity of the channels was abrogated by a TRPC1-targeting blocking antibody T1E3. Conductance of the channels was ~95 pS for outward currents and ~83 pS for inward currents. The channels with similar conductance were also recorded in cells expressing TRPV4–C1 concatamers, in which assembled channels were expected to be mostly 2V4:2C1. Fluorescence Resonance Energy Transfer (FRET) experiments confirmed the formation of a protein complex with 2V4:2C1 stoichiometry while suggesting an unlikeliness of 3V4:1C1 or 1V4:3C1 stoichiometry. Monovalent cation permeability profiles were compared between heteromeric TRPV4–C1 and homomeric TRPV4 channels. For heteromeric TRPV4–C1 channels, their permeation profile was found to fit to Eisenman sequence VI, indicative of a strong field strength cation binding site, whereas for homomeric TRPV4 channels, their permeation profile corresponded to Eisenman sequence IV for a weak field strength binding site. Compared to homomeric TRPV4 channels, heteromeric TRPV4–C1 channels were slightly more permeable to $Ca^{2+}$ and had a reduced sensitivity to extracellular $Ca^{2+}$ inhibition. In summary, we found that, when TRPV4 and TRPC1 were co-expressed in HEK293 cells, the predominate assembly type was 2V4:2C1. The heteromeric TRPV4–C1 channels display distinct electrophysiological properties different from those of homomeric TRPV4 channels.


## 1. Introduction

TRP channels are a superfamily of cation channels that can be divided into seven subfamilies including TRPC, TRPV, and five others. Functional TRP channels are tetrameric complexes consisting of four pore-forming subunits [1], which can be identical (homotetrameric) or different (heterotetrameric) [2–4]. Heteromeric assembly usually occurs between the members within the same TRP subfamily such as between TRPC1 and TRPC5, TRPV5 and TRPV6, TRPM6 and TRPM7 [1,3,5]. However, cross-subfamily heteromerization has also been reported, which includes TRPC1–TRPP2 [6–9] and TRPV4–TRPP2 [10,11].

Recently, we have identified a new type of cross-subfamily heteromeric TRP channels, i.e. TRPV4–C1 channels [12]. The main evidences were as follows: 1) FRET, co-immunoprecipitation and subcellular immunocolocalization methods showed that TRPV4 and TRPC1 could associate with each other to form a physical complex [12]. 2) 4α-PDD and fluid flow, two stimuli that are commonly used to activate TRPV4, could induce $Ca^{2+}$ influx and stimulate cation currents in HEK cells co-expressing TRPV4 and TRPC1. The $Ca^{2+}$ influx and cation currents could be inhibited either by T1E3 [12], which is an antibody targeted at the pore region of TRPC1 and has been shown to inhibit store-operated $Ca^{2+}$ entry in vascular cells [13], or by $TRPC1^{\Delta 567-793}$ [12], which is a mutant with deletion in TRPC1 pore-forming region [14]. These data suggested that the pore regions of TRPC1 and TRPV4 were closely appositioned to each other, likely to form heterotetrameric channels that shared a common pore, similar to those reported for heterotetrameric TRPC1-P2 channels [6].

In the present study, we characterized some basic electrophysiological properties of TRPV4–C1 heteromeric channels, with special emphasis on the channel pore properties including single channel conductance, permeability ratio to different cations, I–V relationship, and voltage-dependent block by extracellular $Ca^{2+}$. Our data show that heteromeric TRPV4–C1 channels have distinct properties that are different from homomeric TRPV4 channels with regard to the relative permeability to monovalent cations, voltage-dependent block by extracellular $Ca^{2+}$.

*Abbreviations:* $[Ca^{2+}]i$, intracellular $Ca^{2+}$ concentration; CFP, cyan fluorescent protein; YFP, yellow fluorescent protein; FRET, Fluorescence Resonance Energy Transfer; 4α-PDD, 4α-phorbol 12,13-didecanoate; TRP, transient receptor potential

* Corresponding author at: School of Biomedical Sciences, The Chinese University of Hong Kong, Hong Kong, China. Tel.: +852 26096877; fax: +852 26035123.
*E-mail address:* yao2068@cuhk.edu.hk (X. Yao).

0005-2736/$ – see front matter © 2011 Elsevier B.V. All rights reserved.
doi:10.1016/j.bbamem.2011.07.049

## 2. Materials and methods

### 2.1. Cell culture

HEK293 cells were cultured in DMEM supplemented with 10% FBS, 100 μg/ml penicillin and 100 U/ml streptomycin.

### 2.2. Cloning and transfection

Human TRPC1 cDNA (NM_003304) was obtained by RT-PCR from human coronary endothelial cells CC2585 (BioWhittaker). $TRPC1^{Mut\text{-}pore}$ was a gift from Dr. Indu Ambudkar, NIH, USA. In this construct, substitutions (Asp→Asn and Glu→Gln) were made at the seven negatively charged residues present in the region between S5 and S6 where TRPC1 pore is located [14]. For FRET, TRPV4 was tagged with CFP or YFP at its C-terminus, and TRPC1 was tagged with CFP or YFP at its C-terminus, TRPV4–C1 concatamer was tagged with CFP or YFP at its C-terminus.

Transfection condition was as described elsewhere [15]. Briefly, HEK293 cells were transfected with various constructs using Lipofectamine 2000. About $6\times10^4$ HEK293 cells were grown in each well of 6-well plates. Transfection was done with 4 μg DNA per plasmid with a total of 4–12 μg plasmid DNA, mixed with 6 μl Lipofectamine 2000 in 200 μl Opti-MEM reduced serum medium in 6-well plates. Unless stated otherwise, the ratio of co-transfected constructs was 1:1. Functional studies were performed 2–3 days post-transfection.

### 2.3. Preparation of T1E3 and preimmune IgG

T1E3 antibody was raised in rabbits using the strategy developed by Xu et al. [13]. Briefly, a peptide corresponding to TRPC1 putative pore-region (CVGIFCEQQSNDTFHSFlGT) was synthesized and conjugated to keyhole limpet hemocyanin (KLH) at Alpha Diagnostic International (USA). The coupled T1E3 peptide (0.5 mg) was injected to the back of a rabbit (day 0), followed by two boost doses at day 21 and day 42 respectively. Antiserum was collected four weeks after the second boost. Immunoglobin G was purified from the T1E3 antiserum using a HiTrap Protein G column (GE Healthcare). For control, pre-immune serum was purified with a HiTrap Protein G column to obtain the immunoglobin G, and then was used in experiments. The applied T1E3 and preimmune IgG were of similar protein quantities in order to balance possible osmotic effect.

### 2.4. Fluorescence Resonance Energy Transfer (FRET) detection

CFP (or YFP)-tagged TRPV4, -tagged TRPC1, and -tagged TRPV4–C1 concatamers were transfected into HEK cells with different combinations. In general, the ratio of co-transfected constructs was 1:1. In experiments where untagged TRPV4 or TRPC1 was used, the ratio of untagged TRPV4 (or TRPC1) vs. CFP-tagged concatamer vs. YFP-tagged concatamer was 4:1:1. FRET signals were detected as described elsewhere [16]. Briefly, an inverted microscope equipped with three-cube FRET filters and CCD camera was used to measure FRET. Three-cube FRET filter cubes were listed as follows (excitation; dichroic; emission): YFP (S500/20 nm; Q515lp; S535/30 nm); FRET (S430/25 nm; 455dclp; S535/30 nm); and CFP (S430/25 nm; 455dclp; S470/30 nm). Average background signal was subtracted. FRET ratio (FR) was calculated by the following equation:

$$FR = \frac{F_{AD}}{F_A} = \frac{\left[S_{FRET}(DA) - R_{D1}{}^{*}S_{CFP}(DA)\right]}{R_{A1}{}^{*}\left[S_{YFP}(DA) - R_{D2}{}^{*}S_{CFP}(DA)\right]}$$

in which $F_{AD}$ represents the total YFP emission with 430/25-nm excitation, and $F_A$ represents the direct YFP emission with 500/20-nm excitation. In $S_{CUBE}$(SPECIMEN), CUBE indicates the filter cube (CFP, YFP, or FRET), and SPECIMEN indicates whether the cell is expressing donor (D, CFP), acceptor (A, YFP), or both (DA). $R_{D1} = (S_{FRET}(D))/(S_{CFP}(D))$, $R_{D2} = (S_{YFP}(D))/(S_{CFP}(D))$, and $R_{A1} = (S_{FRET}(A))/(S_{YFP}(A))$ are predetermined constants that require measurement of the bleed-through of the emission of only CFP- or YFP-tagged molecules into the FRET channel and the emission of only CFP-tagged molecules into the YFP channel.

### 2.5. Whole-cell patch clamp

Whole-cell membrane currents were monitored with an EPC-9 (HEKA Elektronik, Lambrecht, Germany; 8-Pole Bessel filter, 2.9 kHz) using ruptured patches [12]. Patch electrodes had a DC resistance between 2 and 4 mΩ when filled with intracellular solution. Capacitance and access resistance were monitored continuously. Between 50 and 70% of the series resistance was electronically compensated to minimize voltage errors. Pipette and bath solutions were as described [17]. The pipette solution contained in mM: 20 CsCl, 100 $Cs^+$-aspartate, 1 $MgCl_2$, 4 ATP, 0.08 $CaCl_2$, 10 BAPTA, 10 Hepes, pH 7.2. Free intracellular $Ca^{2+}$ was calculated to be ~1 nM for the solution with "webmaxc" available at http://www.stanford.edu/~cpatton/webmaxcS.html [18]. The bath solution contained in mM: 150 NaCl, 6 CsCl, 1 $MgCl_2$, 1.5 $CaCl_2$, 10 glucose, 10 Hepes, pH 7.4. Cells were clamped at 0 mV. I–V relationships were generated by a ramp protocol consisted of a 100-ms linear ramp from −100 mV to +100 mV, repeated every 5 s before and after 4α-PDD. The maximal responses to 4α-PDD were plotted. For the magnitude of 4α-PDD-stimulated currents at +80 mV and/or −80 mV, whole-cell current density (pA/pF) was recorded in response to successive voltage pulses of +80 mV and −80 mV for 100 ms duration. These whole-cell current values were then plotted vs. time to generate a time course. The maximal responses to 4α-PDD were then plotted in bar charts. The currents were sampled at 25 kHz and filtered at 1 kHz. All of the experiments were performed at room temperature (20–23 °C). When needed, cells were pretreated with T1E3 antibody or preimmune IgG for 1 h.

Reversal potential measurement for cation permeability estimation was as described elsewhere [17,19]. The standard extracellular solution contained in mM 150 NaCl, 1 $MgCl_2$, 5 $CaCl_2$, 10 glucose, 10 HEPES, pH 7.4 titrated with NaOH. When indicated in the figure legends, the $Ca^{2+}$ concentration of this solution was varied between 0 and 30 mM. To study the relative permeability of mono- and divalent cations, we used extracellular solutions containing in mM: 1 $MgCl_2$, 10 glucose, 10 HEPES, and either 150 XCl (where X = sodium, cesium, or potassium) or 30 $CaCl_2$ and 120 N-methyl-D-glucamine chloride. These solutions were titrated to pH 7.4 with the appropriate base. The pipette solution contained in mM: 150 NaCl, 1 $MgCl_2$, 4 $Na_2ATP$, 0.037 $CaCl_2$, 5 EGTA, 10 HEPES, pH 7.2 titrated with NaOH, free intracellular $Ca^{2+}$ was calculated to be ~1 nM for the solution. A ramp protocol consisted of a 100-ms linear ramp from −100 mV to +100 mV, repeated every 5 s. 4α-PDD was applied to the extracellular solution at a concentration of 5 μM. The relative permeability of monovalent cations was calculated from the shift in reversal potential after complete substitution of extracellular $Na^+$ by the specific cation [17,19], according to the following equation:

$$P_X / P_{Na} = \exp(\Delta V_{rev} F / RT) \quad (1)$$

where $P_X$ represents the permeability of the monovalent cation. $\Delta V_{rev}$ is the measured shift in reversal potential. Permeability of the $Ca^{2+}$ relative to $Na^+$ was calculated from the absolute reversal potential measured with 30 mM of the $Ca^{2+}$ in the extracellular solution, according to the following equation [17,19]:

$$P_{Ca} / P_{Na} = (1 + \exp(\frac{\Delta V_{rev} F}{RT}))^{*} \frac{([Na]_i + \alpha[Cs]_i)\ \exp(V_{rev} F / RT) - [Na]_e - \alpha[Cs]_e}{4[Ca]_e} \quad (2)$$

where α is $P_{Cs}/P_{Na}$ obtained from Eq. 1, $[Na^+]_e$, $[Na^+]_i$, $[Cs^+]_e$, $[Cs^+]_i$ are the extra- and intracellular concentration of $Na^+$ and $Cs^+$,

respectively. Before calculation of the relative permeability, all reversal potentials were corrected for liquid junction potentials. Note that the current–voltage curves in Figs. 5 and 6 are raw traces without correction for liquid junction potential.

### 2.6. Cell-attached single channel patch clamp

Cell-attached single channel currents were monitored with an EPC-9 (HEKA Elektronik, Lambrecht, Germany), as described elsewhere [20]. Single-channel currents were sampled at 200- and 500-s intervals and filtered at 2 and 1 kHz for HEK293 cells. The pipette solution contained in mM: 150 NaCl, 1 $MgCl_2$, 10 Na–HEPES pH 7.4 and the bath solution was 150 KCl, 5 $MgCl_2$, 10 HEPES, 10 glucose (pH adjusted to 7.4 with KOH). The recordings were made before and after 4α-PDD (5 μM) application. If needed, T1E3 (1:200) or pre-immune IgG (1:200) was introduced into the pipette solution [21–23].

### 2.7. Statistics

Student's *t* test or one-way analysis of variance followed by Newman–Keul's test were used for statistical comparison when appropriate, with probability $p<0.05$ as a significant difference.

## 3. Results

### 3.1. Single channel properties of heteromeric TRPV4–C1 channels

Previous studies using whole-cell patch clamp have demonstrated the existence of heteromeric TRPV4–C1 channels in HEK293 cells co-expressing TRPV4 and TRPC1 [12]. In the present study, we examined the properties of heteromeric TRPV4–C1 channels at single channel level. In cell-attached mode, 4α-PDD (5 μM, a TRPV4 agonist)-activated channels could be detected in cells expressing TRPV4 and those co-expressing TRPV4 and TRPC1 (Fig. 1). In the absence of 4α-PDD, both channels had very little activity. For the channels in TRPV4-expressing cells, application of 4α-PDD (5 μM) increased their open probability (Po) from 0.03 ± 0.01 (n = 6) to 0.71 ± 0.05 (n = 7, Fig. 2A and C). Single channel slope conductance was estimated to be 63 ± 3 pS (n = 7) for inward currents and 85 ± 2 pS (n = 7) for outward currents (Fig. 1D). 4α-PDD (5 μM) also activated the channels in TRPV4–C1 co-expressing cells with Po increased from 0.02 ± 0.01 (n = 6) to 0.73 ± 0.03 (n = 8, Fig. 2B and D). In cells co-expressing TRPV4 and TRPC1, the majority of patches (15 out of 18 patches) contained a channel with single channel slope conductance of 83 ± 2 pS (n = 15) for inward currents and 95 ± 3 pS (n = 15) for outward currents (Fig. 1E). In the minority of patches (3 out of 18), another channel with slightly smaller conductance was recorded, which had conductance of 78 ± 1 pS (n = 3) for inward currents and 86 ± 2 pS (n = 3) for outward currents. A TRPC1-specific blocking antibody T1E3 was used [13]. In this set of experiments, the patch pipettes were backfilled with T1E3 using a two-step protocol [24,25]. T1E3 would slowly diffuse from the pipette onto the membrane, causing a time-dependent inhibition on TRPC1-related channels on cell-attached membrane patches. As expected, T1E3 (1:200) had no effect on the channels in TRPV4-expressing cells, which were presumably homomeric TRPV4 channels (Fig. 2A and C). In contrast, T1E3 (1:200) inhibited the channels in cells co-expressing TRPV4 and TRPC1, suggesting that the channels were heteromeric TRPV4–C1 channels (Fig. 2B and D).

TRPV4–C1 concatamers were constructed. In cells expressing TRPV4–C1 concatamers, the recorded channels had single channel conductance of 84 ± 3 pS (n = 17) for inward currents and 93 ± 3 pS (n = 17) for outward currents (Fig. 1C and F). These values were very similar to the major type of channels recorded from the cells co-expressing individual TRPV4 and TRPC1 (Fig. 1B and E).

### 3.2. Whole-cell properties of heteromeric TRPV4–C1 channels

4α-PDD-stimulated whole-cell currents were examined in cells expressing TRPV4, co-expressing TRPV4 and TRPC1, and expressing TRPV4–C1 concatamers. In all cell types, 4α-PDD-stimulated currents displayed relatively linear current–voltage relationships with a slightly outward rectification at positive voltage when the bath solution contained physiological concentration of mono- and divalent cations (Fig. 3A, B and D). Previously, we have demonstrated that T1E3 could inhibit flow-induced $[Ca^{2+}]_i$ rises in cells co-expressing TRPV4 and TRPC1 [12]. Here the whole-cell patch clamp showed that T1E3 (1:200) incubation for 1 h decreased the 4α-PDD-stimulated whole-cell currents

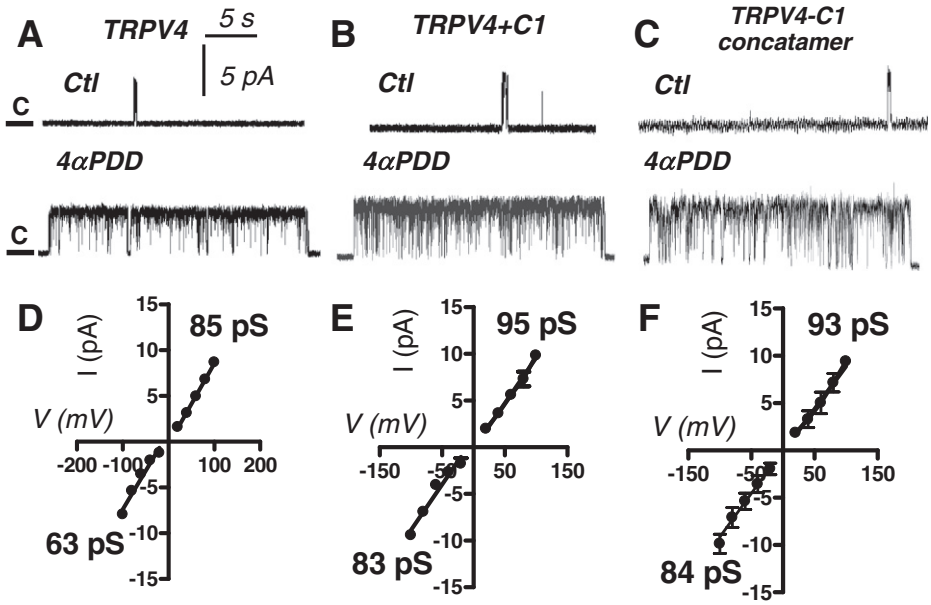


**Fig. 1.** Single channel activity of cell-attached patches from HEK cells expressing different constructs. A and D, HEK cells expressing TRPV4; B and E, HEK cells co-expressing TRPV4 and TRPC1; C and F, HEK cells expressing TRPV4–C1 concatamers. A, B and C, representative single channel traces before (upper panel) and after (lower panel) 5 μM 4α-PDD. The patch membrane was held at +60 mV. Channel close level was marked as *c*. D, E and F, Single channel current–voltage relationships of 4α-PDD-activated single channels in cell-attached patches. Mean ± SEM (*n* = 6–20 patches).

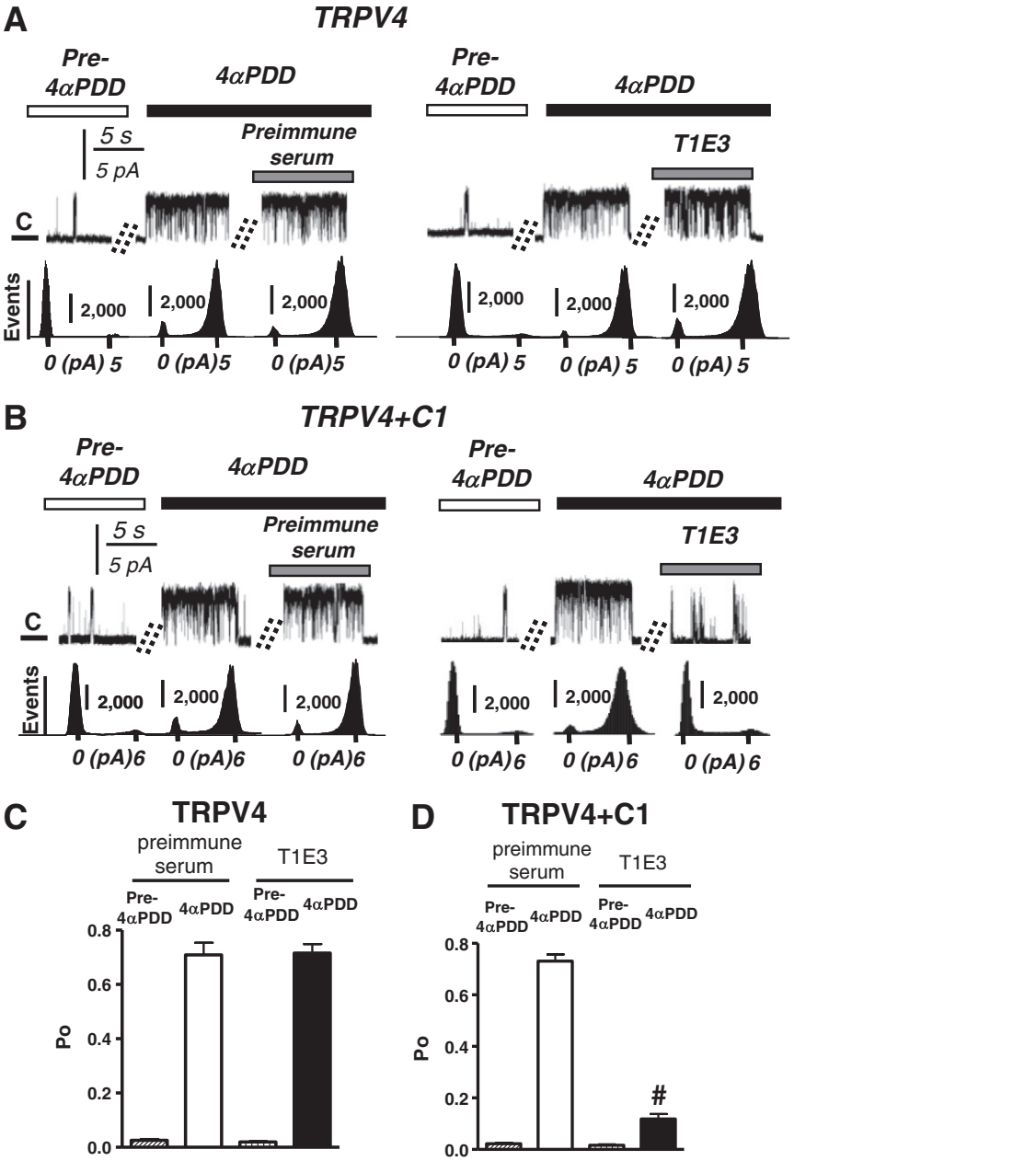


**Fig. 2.** Effect of T1E3 on 4α-PDD-activated single channels in cell-attached patches from HEK cells expressing different constructs. A and C, HEK cells expressing TRPV4; B and D, HEK cells co-expressing TRPV4 and TRPC1. A and B, representative single channel traces. Three traces from left to right represent those "after seal formation", "immediately after 5 μM 4α-PDD", followed by "2 min later after diffusion of T1E3 (1:200) or preimmune IgG (1:200, as control) to the patch membrane". The patch membrane was held at +60 mV. The amplitude histograms of the respective traces are shown under the representative traces. C and D, Single channel open probability ($P_o$) values of 4α-PDD-activated channels in cells expressing TRPV4 (C) and those co-expressing TRPV4 and TRPC1 (D). $P_o$ values were calculated from multiple patches for a 20-s period. Mean ± SEM ($n$ = 6–8 patches). #, $P<0.05$ compared to preimmune IgG with 4α-PDD.

by 83 ± 3% (n = 6) in these cells (Fig. 3C). A TRPC1 pore-dead mutant TRPC1$^{Mut\text{-}pore}$, which carries the point mutations at TRPC1 pore region [14], also drastically reduced the 4α-PDD-stimulated currents by 81 ± 1% (n = 8) in these cells (Fig. 3B and C). Direct application of T1E3 to the bath solution also markedly reduced the 4α-PDD-stimulated whole-cell currents within 2–3 min (Fig. 3E and F).

### 3.3. FRET studies on the stoichiometry of heteromeric TRPV4–C1 channels

FRET was then used to further examine the subunit assembly of TRPV4 and TRPC1. Previously, we have used FRET to demonstrate the physical interaction of TRPV4 and TRPC1 in HEK293 cells co-expressing individual TRPV4 and TRPC1 [12]. Here we found positive FRET signals in cells co-expressing CFP-tagged TRPV4–C1 concatamers and YFP-tagged TRPV4–C1 concatamers (Fig. 4), supporting the formation of channels with 2V4:2C1 stoichiometry. However, no FRET signal was observed in cells co-expressing CFP-tagged TRPV4–C1 concatamers and YFP-tagged TRPV4, or in cells co-expressing CFP-tagged TRPV4–C1 concatamers and YFP-tagged TRPC1 (Fig. 4), suggesting that neither 3V4:1C1 nor 1V4:C1 stoichiometry was favored. These negative data on FRET were not due to the "problem" with YFP-tagged TRPV4 and YFP-tagged TRPC1 constructs, because these two constructs could generate positive FRET signals when paired with CFP-tagged TRPV4 and TRPC1, respectively (Fig. 4). For positive control, significant FRET signals were observed in cells expressing CFP–YFP concatamers (Fig. 4). No FRET signal was detected in a negative control, in which cells were co-transfected with CFP-

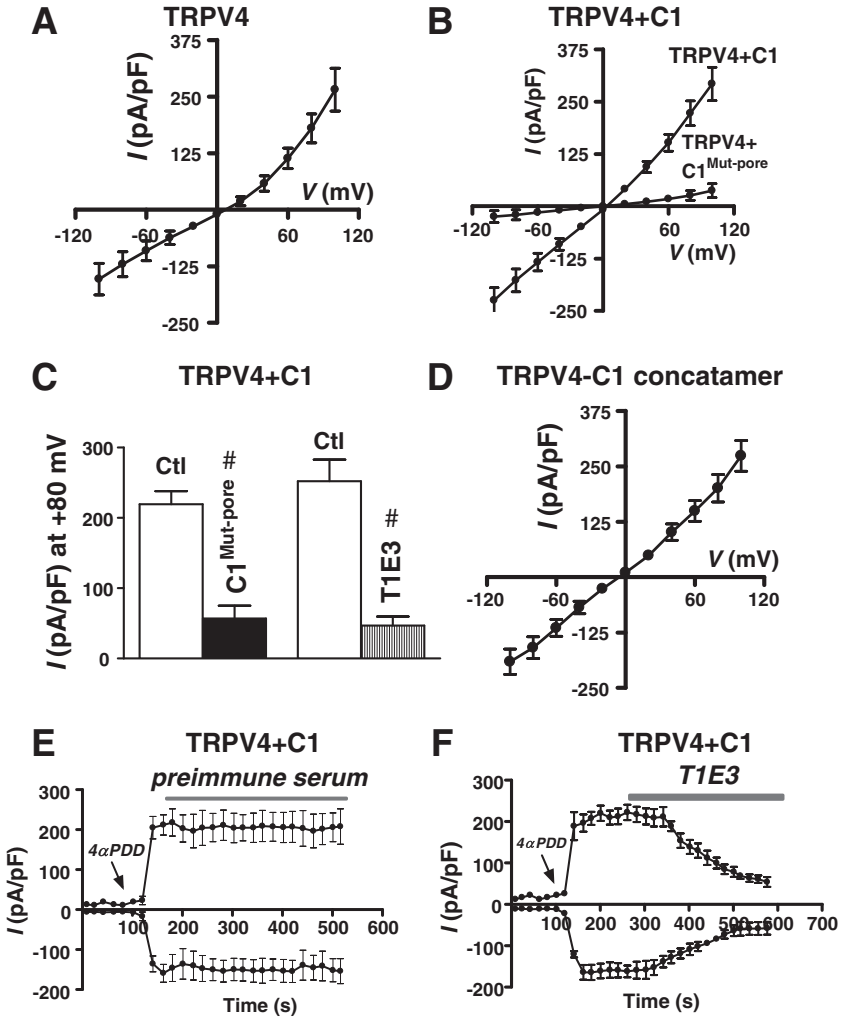


**Fig. 3.** Whole-cell currents of HEK cells expressing different constructs. A, B and D, current–voltage relationships of 4α-PDD-stimulated whole-cell currents for cells expressing TRPV4 (A), co-expressing TRPV4 and TRPC1 (B), and expressing TRPV4–C1 concatamers (D). Cells were clamped at 0 mV. I–V relationships were generated by a ramp protocol consisted of a 100-ms linear ramp from −100 mV to +100 mV. The maximal responses to 4-α-PDD were plotted. C, Data summary showing the effect of TRPC1$^{Mut\text{-}pore}$ and T1E3 on 4α-PDD-stimulated whole-cell cation current at +80 mV in cells co-expressing TRPV4 and TRPC1. In T1E3 series, cells were treated with T1E3 (1:200) or preimmune IgG (1:200, as control) for 1 h at 37 °C before 4α-PDD challenge. In TRPC1$^{Mut\text{-}pore}$ series, HEK cells were co-transfected with TRPV4 plus TRPC1$^{Mut\text{-}pore}$, or with TRPV4 plus TRPC1 as control. E and F, time course of 4α-PDD-stimulated whole-cell current at ±80 mV in cells co-expressing TRPV4 and TRPC1 in response to acute application of preimmune serum (1:100, E) or T1E3 (1:100, F). Values are Mean ± SEM ($n$ = 4–13). #, $P$<0.05 compared to control.

tagged TRPV4 plus YFP-tagged GIRK4 (Fig. 4). GIRK4 belongs to inwardly rectifying potassium channels bearing no similarity to TRP channels, and it served as a membrane protein control.

We also examined whether co-expression of untagged TRPV4 or untagged TRPC1 could interfere the interaction between two V4–C1 concatamers (Fig. 4). The results show that untagged TRPC1 or TRPV4 did not alter the FRET signals generated from the interaction between CFP-tagged TRPV4–C1 concatamers and YFP-tagged TRPV4–C1 concatamers, further supporting the preference and stability of 2V4:2C1 stoichiometry.

### *3.4. Mono- and divalent cation permeability of TRPV4–C1 heteromeric channel*

Relative permeability of homomeric TRPV4 and heteromeric TRPV4–C1 channels to $Na^+$, $Rb^+$, $K^+$, $Li^+$ and $Ca^{2+}$ was estimated based on reverse potential measurement of 4α-PDD-stimulated cation currents using the methods established previously [17]. After full activation of the currents with 4α-PDD (5 μM), extracellular solutions were switched to the ones that contain different permeant cation species, for example from $K^+$-containing to $Cs^+$-containing bath solution. The relative permeability was then calculated from the shifts in the reversal potential. The results showed that TRPV4 was moderately selective for $Ca^{2+}$ over $Na^+$ ions with $P_{Ca}$:$P_{Na}$ = *7.1*:*1* (Fig. 5D), and its relative permeability sequences for monovalent cations were $P_K$:$P_{Rb}$:$P_{Cs}$:$P_{Na}$:$P_{Li}$ = *1.42*:*1.31*:*1.28*:*1*:*0.79* (Fig. 5A), corresponding to Eisenman sequence IV. In contrast, the channels recorded from cells co-expressing individual TRPV4 and TRPC1 and those expressing TRPV4–C1 concatamers were more permeable to $Ca^{2+}$ with $P_{Ca}$:$P_{Na}$ = *9.2*:*1* and *9.3*:*1*, respectively (Fig. 5E and F). The monovalent cation permeability of the latter two was very close, with $P_K$:$P_{Na}$:$P_{Rb}$:$P_{Cs}$:$P_{Li}$ = *1.44*:*1*:*0.93*:*0.77*:*0.68* for cells co-expressing individual TRPV4 and TRPC1 and *1.46*:*1*:*0.95*:*0.79*:*0.68* for cells expressing TRPV4–C1 concatamers (Fig. 5B and C), both corresponding to Eisenman sequence VI.

Met-680 of TRPV4 is a crucial residue positioned at the pore region of TRPV4 (17). Conversion of Met-680 to aspartic acid caused a drastic reduction in current density for cells expressing TRPV4 or co-expressing TRPV4 and TRPC1 (Fig. 5J). After replacing TRPV4 with TRPV4$^{M680D}$, switching extracellular solution from a $Na^+$-containing solution to a $Ca^{2+}$ (30 mM)-containing solution as the sole permeant cation caused a leftward shift of the reversal potential corresponding

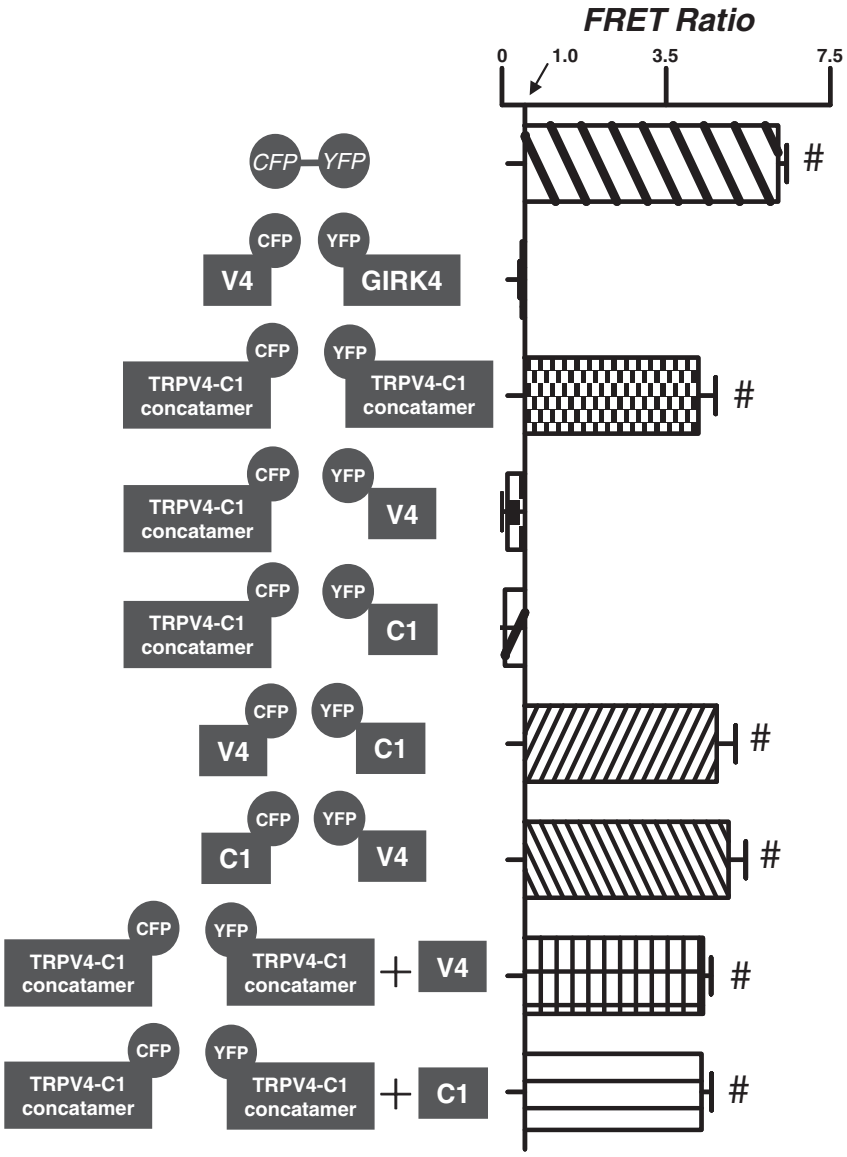


**Fig. 4.** FRET detection by three-cube FRET in HEK cells expressing different constructs. Horizontal axes indicate FRET ratio (FR) of living HEK cells expressing indicated constructs. FR = 1, no FRET. FR > 1, having FRET. Mean ± SEM ($n$ = 20–35). #, $P$ < 0.05 compared to negative control (CFP-tagged TRPV4 plus YFP-tagged GIRK4).

to a $P_{Ca}/P_{Na}$ value ≪ 1 (Fig. 5H and I), suggesting that conversion of Met-680 to aspartic acid abolished the $Ca^{2+}$ permeability of both homomeric TRPV4 and heteromeric TRPV4–C1 channels.

### 3.5. Voltage-dependent inhibition of TRPV4–C1 heteromeric channels by extracellular $Ca^{2+}$

It was reported that extracellular $Ca^{2+}$ caused a voltage-dependent inhibition on homomeric TRPV4 channels [17]. This was confirmed in the present study. In the absence of divalent cations, the current–voltage relation of homomeric TRPV4 was linear (Fig. 6A). Extracellular $Ca^{2+}$ caused a concentration-dependent inhibition of the currents that was more pronounced at negative potentials, characteristic of a voltage-dependent block (Fig. 6A). However, for cells co-expressing TRPV4 and TRPC1 and for those expressing TRPV4–C1 concatamers, the voltage-dependent blockage by extracellular $Ca^{2+}$ was much smaller than that of homomeric TRPV4 channels (Fig. 6B and C). This was especially evident at negative membrane potential. At −80 mV, 30 mM extracellular $Ca^{2+}$ only reduced the whole-cell currents by 46 ± 7% (n = 6) for cells expressing TRPV4–C1 concatamers (Fig. 6C and D) and 46 ± 4% (n = 4) for those co-expressing individual TRPV4 and TRPC1 (Fig. 6B and D), respectively. In contrast, the same concentration of extracellular $Ca^{2+}$ reduced the current density of homomeric TRPV4 channels by a much large degree of 74 ± 8% (n = 5) (Fig. 6A and D).

## 4. Discussion

Recently, we have found a novel type of cross-subfamily heteromeric channels, TRPV4–C1 channels [12]. In the present study, we characterized some basic electrophysiological properties of this heteromeric TRPV4–C1 channels. The major type of channels in cells co-expressing TRPV4 and TRPC1 had single channel conductance of 83 pS for inward currents and 95 pS for outward currents. It is likely that this channel type represents 2V4:2C1 stoichiometry. When compared to homomeric TRPV4 channels, these heteromeric TRPV4–C1 channels were slightly more permeable to $Ca^{2+}$, displayed different monovalent permeation profile, and had a reduced sensitivity to extracellular $Ca^{2+}$ inhibition.

4α-PDD-activated channels recorded from the cells co-expressing TRPV4 and TRPC1 were not very different from homomeric TRPV4 in terms of their single channel conductance (~95 pS vs. ~85 pS for

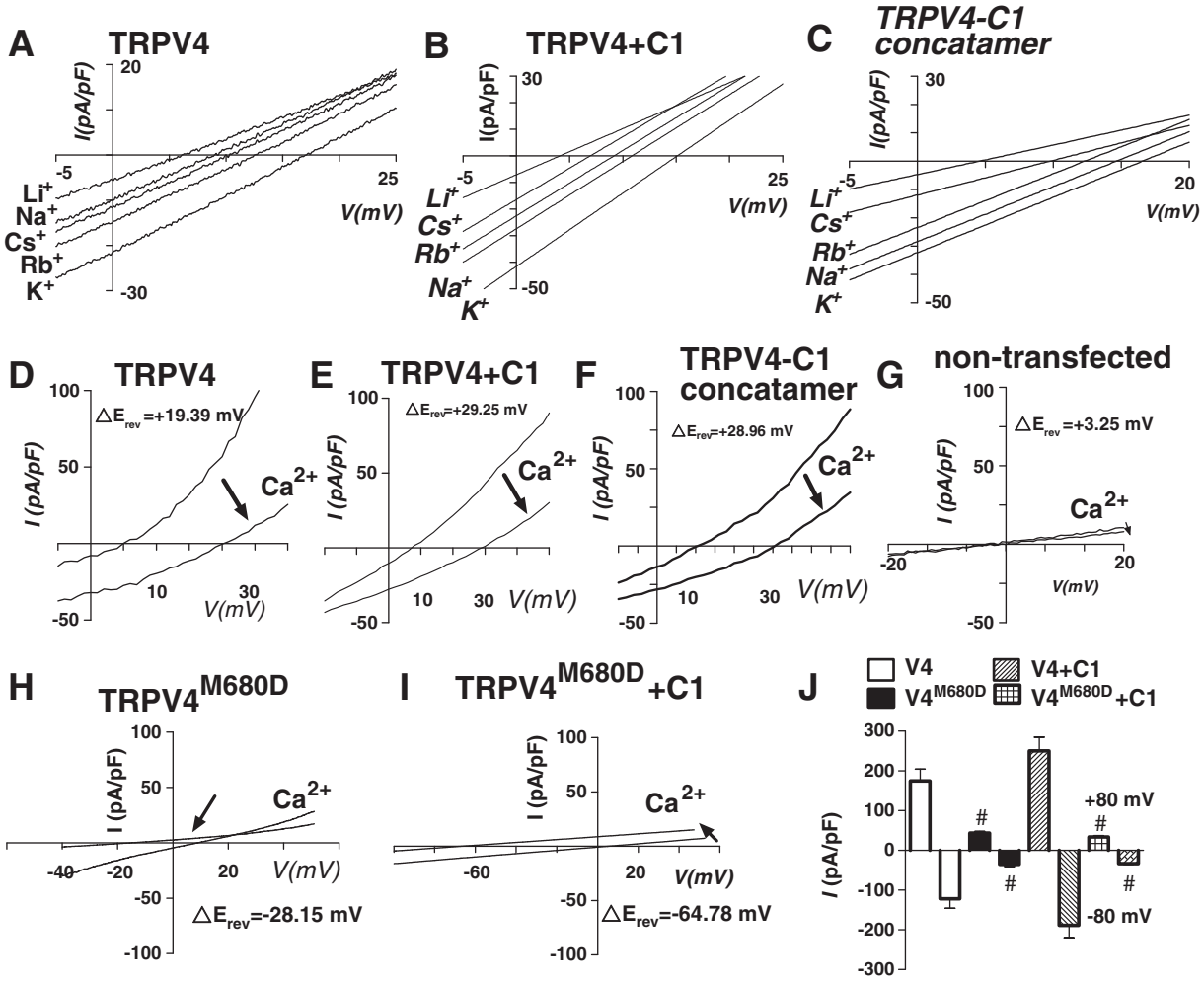


**Fig. 5.** Cation permeability sequence of HEK cells expressing different constructs. A–C, the monovalent currents in cells expressing indicated constructs. Extracellular solutions contained 150 mM of the indicated monovalent cation as sole charge carrier. D–I, $Ca^{2+}$ permeability in cells expressing indicated constructs. Extracellular solutions changed from standard extracellular solution to the one containing 30 mM $Ca^{2+}$ as the sole charge carrier (arrow). In panel D–G, the resultant shift in reversal potential is indicated. A and D, cells expressing TRPV4; B and E, cells co-expressing TRPV4 and TRPC1; C and F, cells expressing TRPV4-C1 concatamers; G, non-transfected HEK cells; H, cells expressing $TRPV4^{M680D}$; I, cells co-expressing $TRPV4^{M680D}$ and TRPC1. Each trace was representative from 6 to 7 individual cells. J, Summary for the magnitude of maximal 4α-PDD-stimulated whole-cell current density at the membrane voltage of +80 mV and −80 mV for cells expressing indicated constructs. Mean ± SEM ($n = 4$–15). #, $P<0.05$ compared to those contained wild-type TRPV4.

outward current). In comparison, the single channel conductance of homomeric TRPC1 was reported to be at ~16 pS [26]. One may wonder whether the recorded channels from the cells co-expressing TRPV4 and TRPC1 indeed represented heteromeric TRPV4–C1 channels or they were just homomeric TRPV4. A TRPC1-specific blocking antibody T1E3 was used to differentiate these two possibilities. T1E3 targeted against the ion permeation pore of TRPC1 channels [13], therefore T1E3 was expected to inhibit heteromeric TRPV4–C1 channels but not homomeric TRPV4. Our results showed that the channels were inhibited by T1E3, suggesting that they were indeed heteromeric TRPV4–C1 channels. In whole-cell patch recordings, T1E3 and a TRPC1 pore-dead mutant $TRPC1^{Mut\text{-}pore}$ each reduced 4α-PDD-stimulated whole-cell currents by ≥80%, even though TRPC1 and TRPV4 were transfected to the cells at a molecular ratio of 1:1. These results suggested the relative abundance of heteromeric TRPV4–C1 vs. homomeric TRPV4 of at least 4:1 in these cells. This ratio of 4:1 could be underestimated because these treatments were not expected to fully abolish TRPV4–C1-mediated currents. Note that only 4α-PDD-activated channels were studied here. Homomeric TRPC1 could not be activated by 4α-PDD, thus were not studied here.

Heteromeric TRPV4–C1 channels could have different subunit stoichiometry including 3V4:1C1, 2V4:2C1, and 1V4:3C1. It would be interesting to know which assembly type may dominate. To address this question, TRPV4–C1 concatamers were constructed. It was expected that the expression of TRPV4–C1 concatamers would mostly result in the formation of channels with 2V4:2C1 stoichiometry, assuming that the contribution of endogenous TRPV4 and TRPC1 was small. Previous studies reported that the expression of TRPV4 and TRPC1 in non-transfected HEK293 cells was indeed very low [12]. In the present study, 4α-PDD-activated single channels were recorded in cells expressing TRPV4–C1 concatamers, and the channels were found to be very close to the major type of channels in cells co-expressing individual TRPV4 and TRPC1 with regards to single channel conductance. Importantly, FRET studies confirmed the formation of protein complex with 2V4:2C1 stoichiometry while suggesting the unlikeliness of 3V4:1C1 or 1V4:3C1 stoichiometry. Therefore, it was likely that the main assembly type in cells co-expressing individual TRPV4 and TRPC1 was 2V4:2C1. However, it should be noted that there was a minority type of channels with relatively smaller conductance (78 pS for inward currents and 86 pS for outward currents) presented in cells co-expressing individual TRPV4 and TRPC1. Those could represent the channels with other subunit stoichiometries such as 3V4:1C1 or 1V4:3C1. One point to consider is that 1V4:3C1 stoichiometry has only one V4 subunit, which may or may not be sufficient for 4α-PDD response. Regardless of their exact stoichiometry, low abundance of these channels made it difficult to

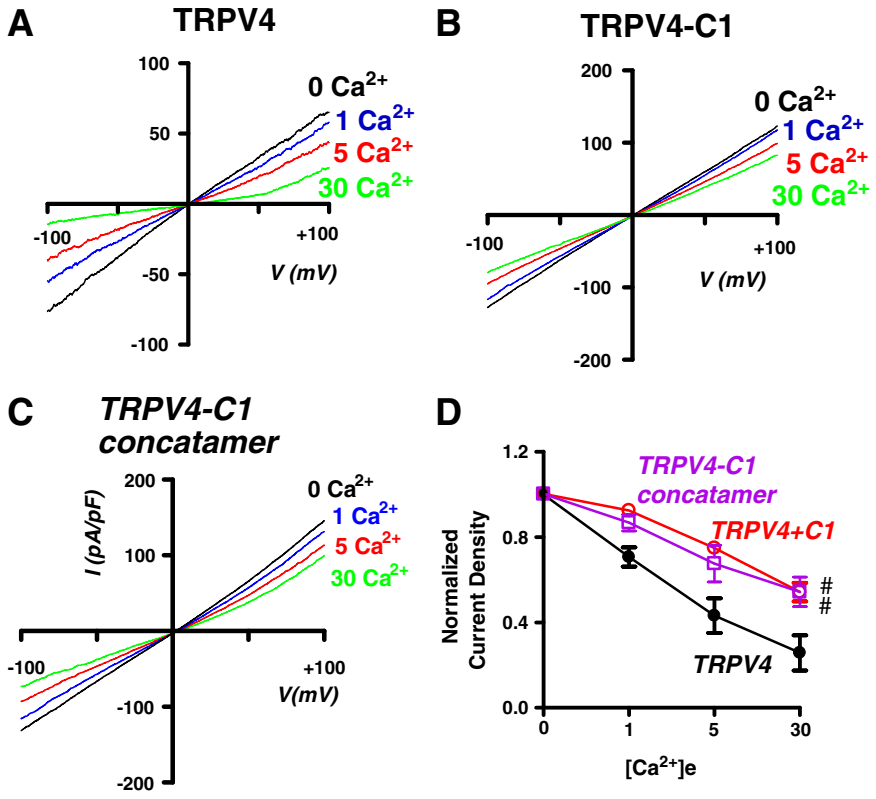


**Fig. 6.** $Ca^{2+}$-dependent rectification of whole-cell currents in cells expressing different constructs. A–C, current–voltage relationships of 4α-PDD-stimulated whole-cell cation currents for cells expressing TRPV4 (A), co-expressing TRPV4 and TRPC1 (B), and expressing TRPV4–C1 concatamers (C). Extracellular solution contained the indicated $Ca^{2+}$ concentrations. Note the appearance of inward and outward rectification in the presence of $Ca^{2+}$. D, Data summary showing concentration-dependent inhibition by extracellular $Ca^{2+}$ at −80 mV in cells expressing indicated constructs. The currents were normalized to the values in $Ca^{2+}$-free extracellular bath (D). Values are Mean ± SEM ($n$ = 4–6). #, $P$<0.05 compared to TRPV4.

further characterize the channels. Thus we were not able to determine whether this minority type of channels were also sensitive to T1E3 inhibition. Low abundance could also explain why we failed to detect positive FRET signals for these types of stoichiometries. It is possible that these types of heteromerization may be below the detection limits of our FRET experiments. Our conclusion of 2V4:2C1 stoichiometry appears to agree with several recent reports, which demonstrated the same 2:2 subunit stoichiometry for two other cross-subfamily TRP channels, i.e., heteromeric TRPV4-P2 and heteromeric TRPC1-P2 channels [9,11].

Previous studies showed that homomeric TRPV4 has a weak $Ca^{2+}$ selectivity over $Na^{+}$ with the relative permeability ratio of $P_{Ca}$:$P_{Na}$ = *6.9*:*1*, and its monovalent permeation profile corresponds to Eisenman sequence IV, indicating a weak field strength cation binding site [17,27]. This was confirmed by the present study, in which we showed relative cation permeability ratio of $P_{Ca}$:$P_K$:$P_{Cs}$:$P_{Na}$ = *7.1*:*1.4*:*1.2*:*1* for homomeric TRPV4, similar to the reported value (17). In comparison, the channels recorded from cells co-expressing TRPV4–C1 channels and those expressing TRPV4–C1 concatamers were slightly more selective for $Ca^{2+}$ with $P_{Ca}$:$P_{Na}$ = *9.2*:*1*, and displayed different monovalent permeation profile of Eisenman sequence VI, indicative of a strong field strength cation binding site. Previous evidence suggested that Met-680 of TRPV4 was crucial for the proper functioning of the TRPV4 pore [17]. Introducing a negative charge at this position (M680D) was found to cause a reduction in current density and a complete loss of $Ca^{2+}$ permeation [17]. In the present study, we found that conversion of Met-680 to aspartic acid (D) also reduced the $Ca^{2+}$ permeability of heteromeric TRPV4–C1 channels. These data suggested that $Met^{680}$ was not only crucial for the proper functioning of homomeric TRPV4 pore, but also important for the proper functioning of heteromeric TRPV4–C1 pore. Another marked difference between homomeric TRPV4 and heteromeric TRPV4–C1 was their sensitivity to extracellular $Ca^{2+}$ inhibition. We found that extracellular $Ca^{2+}$ inhibited heteromeric TRPV4–C1 at a much less degree comparing to its inhibition on homomeric TRPV4.

In conclusion, the present study demonstrated that, in HEK cells co-expressing TRPV4 and TRPC1, the predominate assembly type was the heteromeric channels with stoichiometry of 2TRPV4:2TRPC1. Different from homomeric TRPV4, these heteromeric TRPV4–C1 channels have reduced sensitivity to extracellular $Ca^{2+}$ inhibition and display different monovalent permeation profile.

## Acknowledgements

We thank Dr. Ambudkar I (NIH, USA) for $TRPC1^{Mut\text{-}pore}$. This work was supported by CUHK477408, CUHK479109 and CUHK478710 from the Hong Kong RGC, Focused Investment Scheme C and Group Research Grant of CUHK.

## References

[1] J.G. Hoenderop, T. Voets, S. Hoefs, F. Weidema, J. Prenen, B. Nilius, R.J. Bindels, Homo- and heterotetrameric architecture of the epithelial $Ca^{2+}$ channels TRPV5 and TRPV6, EMBO J. 22 (2003) 776–785.
[2] T. Hofmann, M. Schaefer, G. Schultz, T. Gudermann, Subunit composition of mammalian transient receptor potential channels in living cells, Proc. Natl. Acad. Sci. U. S. A 99 (2002) 7461–7466.
[3] C. Strubing, G. Krapivinsky, L. Krapivinsky, D.E. Clapham, TRPC1 and TRPC5 form a novel cation channel in mammalian brain, Neuron 29 (2001) 645–655.
[4] G.D. Smith, M.J. Gunthorpe, R.E. Kelsell, P.D. Hayes, P. Reilly, P. Facer, J.E. Wright, J.C. Jerman, J.P. Walhin, L. Ooi, J. Egerton, K.J. Charles, D. Smart, A.D. Randall, P. Anand, J.B. Davis, TRPV3 is a temperature-sensitive vanilloid receptor-like protein, Nature 418 (2002) 186–190.
[5] P.K. Lepage, G. Boulay, Molecular determinants of TRP channel assembly, Biochem. Soc. Trans. 35 (2007) 81–83.

[6] C.X. Bai, A. Giamarchi, L. Rodat-Despoix, F. Padilla, T. Downs, L. Tsiokas, P. Delmas, Formation of a new receptor-operated channel by heteromeric assembly of TRPP2 and TRPC1 subunits, EMBO Rep. 9 (2008) 472–479.
[7] L. Tsiokas, T. Arnould, C. Zhu, E. Kim, G. Walz, V.P. Sukhatme, Specific association of the gene product of PKD2 with the TRPC1 channel, Proc. Natl. Acad. Sci. U. S. A 96 (1999) 3934–3939.
[8] P. Zhang, Y. Luo, B. Chasan, S. Gonzalez-Perrett, N. Montalbetti, G.A. Timpanaro, M.R. Cantero, A.J. Ramos, W.H. Goldmann, J. Zhou, H.F. Cantiello, The multimeric structure of polycystin-2 (TRPP2): structural–functional correlates of homo- and hetero-multimers with TRPC1, Hum. Mol. Genet. 18 (2009) 1238–1251.
[9] T. Kobori, G.D. Smith, R. Sandford, J.M. Edwardson, The transient receptor potential channels TRPP2 and TRPC1 form a heterotetramer with a 2:2 stoichiometry and an alternating subunit arrangement, J. Biol. Chem. 284 (2009) 35507–35513.
[10] M. Kottgen, B. Buchholz, M.A. Garcia-Gonzalez, F. Kotsis, X. Fu, M. Doerken, C. Boehlke, D. Steffl, R. Tauber, T. Wegierski, R. Nitschke, M. Suzuki, A. Kramer-Zucker, G.G. Germino, T. Watnick, J. Prenen, B. Nilius, E.W. Kuehn, G. Walz, TRPP2 and TRPV4 form a polymodal sensory channel complex, J. Cell Biol. 182 (2008) 437–447.
[11] A.P. Stewart, G.D. Smith, R.N. Sandford, J.M. Edwardson, Atomic force microscopy reveals the alternating subunit arrangement of the TRPP2–TRPV4 heterotetramer, Biophys. J. 99 (2010) 790–797.
[12] X. Ma, S. Qiu, J. Luo, Y. Ma, C.Y. Ngai, B. Shen, C.O. Wong, Y. Huang, X. Yao, Functional role of vanilloid transient receptor potential 4-canonical transient receptor potential 1 complex in flow-induced $Ca^{2+}$ influx, Arterioscler. Thromb. Vasc. Biol. 30 (2010) 851–858.
[13] S.Z. Xu, D.J. Beech, TrpC1 is a membrane-spanning subunit of store-operated $Ca^{2+}$ channels in native vascular smooth muscle cells, Circ. Res. 88 (2001) 84–87.
[14] X. Liu, B.B. Singh, I.S. Ambudkar, TRPC1 is required for functional store-operated $Ca^{2+}$ channels. Role of acidic amino acid residues in the S5–S6 region, J. Biol. Chem. 278 (2003) 11337–11343.
[15] H.Y. Kwan, B. Shen, X. Ma, Y.C. Kwok, Y. Huang, Y.B. Man, S. Yu, X. Yao, TRPC1 associates with $BK_{Ca}$ channel to form a signal complex in vascular smooth muscle cells, Circ. Res. 104 (2009) 670–678.
[16] S. Qiu, Y.L. Hua, F. Yang, Y.Z. Chen, J.H. Luo, Subunit assembly of N-methyl-D-aspartate receptors analyzed by Fluorescence Resonance Energy Transfer, J. Biol. Chem. 280 (2005) 24923–24930.
[17] T. Voets, J. Prenen, J. Vriens, H. Watanabe, A. Janssens, U. Wissenbach, M. Bodding, G. Droogmans, B. Nilius, Molecular determinants of permeation through the cation channel TRPV4, J. Biol. Chem. 277 (2002) 33704–33710.
[18] A. Muller, M. Kukley, M. Uebachs, H. Beck, D. Dietrich, Nanodomains of single $Ca^{2+}$ channels contribute to action potential repolarization in cortical neurons, J. Neurosci. 27 (2007) 483–495.
[19] G. Owsianik, K. Talavera, T. Voets, B. Nilius, Permeation and selectivity of TRP channels, Annu. Rev. Physiol 68 (2006) 685–717.
[20] H. Watanabe, J. Vriens, J. Prenen, G. Droogmans, T. Voets, B. Nilius, Anandamide and arachidonic acid use epoxyeicosatrienoic acids to activate TRPV4 channels, Nature 424 (2003) 434–438.
[21] J. Fauconnier, J.T. Lanner, A. Sultan, S.J. Zhang, A. Katz, J.D. Bruton, H. Westerblad, Insulin potentiates TRPC3-mediated cation currents in normal but not in insulin-resistant mouse cardiomyocytes, Cardiovasc. Res. 73 (2007) 376–385.
[22] A.P. Albert, V. Pucovsky, S.A. Prestwich, W.A. Large, TRPC3 properties of a native constitutively active $Ca^{2+}$-permeable cation channel in rabbit ear artery myocytes, J. Physiol 571 (2006) 361–369.
[23] J. Chen, R.F. Crossland, M.M. Noorani, S.P. Marrelli, Inhibition of TRPC1/TRPC3 by PKG contributes to NO-mediated vasorelaxation, Am. J. Physiol Heart Circ. Physiol 297 (2009) H417–H424.
[24] A. Auerbach, Single-channel dose–response studies in single, cell-attached patches, Biophys. J. 60 (1991) 660–670.
[25] Y. Ohya, N. Adachi, Y. Nakamura, M. Setoguchi, I. Abe, M. Fujishima, Stretch-activated channels in arterial smooth muscle of genetic hypertensive rats, Hypertension 31 (1998) 254–258.
[26] B. Nilius, G. Owsianik, T. Voets, J.A. Peters, Transient receptor potential cation channels in disease, Physiol Rev. 87 (2007) 165–217.
[27] G. Eisenman, R. Horn, Ionic selectivity revisited: the role of kinetic and equilibrium processes in ion permeation through channels, J. Membr. Biol. 76 (1983) 197–225.